Diffusion Tensor Magnetic Resonance Imaging of Prostate Cancer

Guglielmo Manenti, MD, Marco Carlani, MD, Stefano Mancino, MD, Vittorio Colangelo, MD, Mauro Di Roma, MD, Ettore Squillaci, MD, and Giovanni Simonetti, MD, PhD

Purpose: To explore the feasibility of 3T magnetic resonance (MR) diffusion tensor imaging (DTI) and fiber tracking (FT) in patients with prostate cancer.

Materials and methods: Thirty consecutive patients (mean age, 62.5 years) with biopsy proven prostate cancer underwent 3T-MR imaging (MRI) and DTI using a 6-channel external phased-array coil before radical prostatectomy. Regions of interest of 14 pixels were defined in tumors and nonaffected areas in the peripheral zone (PZ) and central gland (CG), according to histopatology after radical prostatectomy. Apparent diffusion coefficient (ADC) and fractional anisotropy (FA) values were determined. Differences in mean ADC and FA values among prostate cancer, normal PZ and CG were compared by 2-sided Student *t* test. The predominant diffusion direction of the prostate anisotropy was color coded on a directionally encoded color (DEC) map. A 3D reconstruction of fiber tract orientations of the whole prostate was determined using the continuous tracking method. The overall image quality for tumor localization and local staging was assessed in retrospective matching with whole-mount section histopathology images. Nodules detected at MRI were classified as matched lesions if tumor presence and extension were evidenced at histopathology.

Results: For all the patients, the DTI sequence images were suitable for the evaluation of the zonal anatomy of the prostate gland and the tumor localization. Quantitative evaluation of the regions of interest (ROIs) showed a mean ADC value significantly lower in the peripheral neoplastic area ($1.06 \pm 0.37 \times 10^{-3}$ mm^2/s) than in the normal peripheral portion ($1.95 \pm 0.38 \times 10^{-3}$ mm^2/s) ($P < 0.05$). The mean FA values calculated in the normal peripheral (0.47 ± 0.04) and central area (0.41 ± 0.08) were very similar ($P > 0.05$). The mean FA values in the neoplastic lesion (0.27 ± 0.05) were significantly lower ($P < 0.05$) than in the normal peripheral area and in the normal central and adenomyomatous area. DEC map showed a top-bottom type preferential direction in the peripheral but not in the central area, with the tumor lesions reducing the diffusion coding direction represented as color zones tending toward gray. Tractographic analysis permitted good delineation of the prostate anatomy (capsule outline, peripheral and central area borders) and neoplastic lesion extension and capsule infiltration compared with histopathology.

Conclusions: Three Tesla DTI of the prostate gland is feasible and has the potential for providing improved diagnostic information.

Key Words: 3 Tesla, diffusion tensor, magnetic resonance imaging, tractography

(*Invest Radiol* 2007;42: 412–419)

Prostate cancer is the most common type of cancer in the American male population, causing an estimated 11.5% death rate per year.[1] A similar trend is recorded in Europe where the rate of prostate cancer is 55 cases/100,000 and the mortality rate 22.6 deaths/100,000.[2]

To date the best available technique for localizing and staging prostate cancer is magnetic resonance (MR) performed with an endorectal coil in association with a phased-array pelvic coil. Combining T2 weighted (T2W) imaging with MR spectroscopy and dynamic MR imaging (MRI), high spatial resolution images of the prostate can be obtained and it is possible to evaluate local metastases.[3,4] Recently, Tanimoto et al[5] reported that prostate cancer can be accurately detected by combining diffusion weighted (DWI) and dynamic MRI with T2W imaging. In another study Miao et al demonstrated that at the 3T-MRI, DWI is superior to T2W in detecting prostate cancer.[6] The success of DWI is strictly correlated to the concept that the water molecules, interacting with cell membranes and macromolecules during their incoherent movement, provide important information on the microscopic organization of the tissue.

In general, in tissues without a well-ordered microstructure, the water molecules flow in an isotropic way, ie, in an identical way in the different spatial directions.[7] On the other hand, in structures with a high degree of structural order, molecular diffusion has a preferential direction or anisotropy. The change in diffusion flow in terms of intensity and direction occurs, therefore, in a 3-dimensional way.[7–9]

The application of DWI was initially applied only to the study of the brain.[10–12] With the recent introduction of the ultra-fast echo-planar sequences, DWI has been applied also to the evaluation of abdominal and pelvic pathology.[13–19]

Previous studies have described the application of diffusion tensor imaging (DTI) in the myocardium and more

Received September 22, 2006, and accepted for publication, after revision, March 6, 2007

From the Department of Diagnostic Imaging and Interventional Radiology, University of "Tor Vergata," Rome, Italy.

Reprints: Guglielmo Manenti, MD, Department of Diagnostic Imaging and Interventional Radiology, Università degli Studi di Roma "Tor Vergata," Viale Oxford, 81-00133 Rome, Italy. E-mail: guggi@tiscali.it.

ISSN: 0020-9996/07/4206-0412

recently in the kidney.[20,21] Sinha et al carried out a prostatic preliminary DTI study in 6 healthy volunteers, confirming the architectural anisotropy of the gland and opening up the possibility of early identification of the structural changes related to the development of the disease.[22]

DTI can be calculated with magnetic fields of 1.5T, however, with a limit imposed by the strength of the signal obtained from the water molecule diffusion flow. The conspicuous increase in signal-noise ratio (SNR) that occurs with a 3T-MR should permit a noticeable improvement in the evaluation of this phenomenon.

To date, numerous studies have shown the applicability of the tractographic analysis in the study of the normal and pathologic central nervous system.[23–25] However, it is theoretically possible to apply this technique to any type of tissue with a fibrous structure, characterized by anisotropy. Promising studies in this respect were directed toward the evaluation of the striated skeletal musculature.[26]

In our study we present preliminary results of the quantitative evaluation of 3T-MR DTI in discriminating between normal and neoplastic prostate tissue.

The tractographic process was also applied to obtain both a 3-dimensional view of the gland and its changes related to the presence of the neoplastic lesion.

MATERIALS AND METHODS

Patient Population

Between March and November 2005, 30 patients with elevated serum prostate-specific antigen (PSA) and histologically confirmed prostate cancer, underwent a presurgical staging evaluation by MR examination 6 weeks after the biopsy.

The patients' mean age was 62.5 years (range 56–69 years) with a mean serum PSA value of 7 ng/mL (range 3.0–35.0 ng/mL) and the mean Gleason score on postbiopsy analysis of 7 (range 5–9). All patients were administered 30 mg of butylscopolamine iv (Buscopan. Boehringer, Ingelheim, Germany) 5 minutes before the examination, to reduce the intestinal peristalsis. Informed consent was obtained from all patients, and the protocol was approved by the institutional review board.

MR Imaging

All the MR images were obtained with a 3T scanner (Intera Achieva, Philips Medical Systems, Best, The Netherlands) equipped with 80 mT/m maximum width and 200 mT/m/ms slew rate gradients, using a 6-channel phased-array pelvic receiver coil fixed by an elastic strip to the patient's body to limit respiratory artifacts.

The morphologic study of the prostate cavity was carried out after a multiplanar centering sequence (half-Fourier single shot turbo spin echo, HASTE) to correctly position the coil.

Images were obtained with a high spatial resolution T2W turbo spin echo (TSE) technique (TR/TE 3295/150 milliseconds, slice thickness 3 mm, gap 0.3 mm, number of signal averages [NSA] 6, field of view [FOV] 160 mm, flip angle 90°, matrix 720 × 720 with an in-plane voxel dimension of 0.22 mm × 0.22 mm; scan time 5.56 minutes) on the 3 planes including the whole prostate and seminal vesicles. A long TE was used to obtain the most T2 contrast of the peripheral gland.

The morphologic evaluation was completed with an axial-T1W TSE (TR/TE 469/11 milliseconds, slice thickness 3 mm, gap 0.3 mm, NSA 3, FOV 160 mm, flip angle 90°, matrix 256 × 512; scan time 4.53 minutes) to show the possible presence of hemoglobin degradation products, as a result of the previous biopsies.

A radiologist expert in prostate imaging (G.M.) identified the areas suspicious for neoplasia characterized by low signal intensity on the T2W imaging (focal hypointensity T2W area ≥5 mm in diameter). These were then included in the acquisition volume of multislice DTI.

MR Diffusion Tensor Imaging

A spin-echo echo-planar (SE-EPI) single shot multislice DTI sequence was used [TR/TE 2500/49 milliseconds, NSA 10, slice number 8, slice thickness 3 mm, gap 0.3 mm, matrix 80 × 120, FOV 160 mm, nominal voxel dimension 1.3 mm × 1.3 mm, b-values 2 (0, 1000 s/mm^2), scan time 5.15 minutes]. A high b-value was chosen to reduce the "pseudodiffusion" effects of the glandular blood flow. Diffusion sensitization was obtained by applying 2 symmetrical diffusion gradient pulses before and after the 180° pulse of the spin echo sequence (motion sensitizing gradients). The diffusion sensitization gradients were applied along 6 different directions indicated by the vectors (x, y, z):[(0,0,1), (0,1,0), (1,0,0), (0, $1/\sqrt{2}$, $1/\sqrt{2}$), ($1/\sqrt{2}$, 0, $1/\sqrt{2}$), ($1/\sqrt{2}$, $1/\sqrt{2}$, 0)] using the following convention: x (phase coding, upper-lower), y (readout, anterior-posterior), z (layer selection, left-right) as suggested by Pierpaoli et al.[27]

The acquisition volume was placed on the axial plane, on the basis of the T2W images, carefully including the low signal suspicious areas.

The echo-planar sequence also included a fat suppression pulse. The morphologic acquisitions and the DTI were carried out with a parallel SENSE (sensitivity encoding) imaging technique, using a reduction factor of 2.[28,29]

The duration of the entire protocol of morphologic and functional imaging, including patient preparation and positioning, was approximately 30 minutes.

Regions of interest (ROIs) positioning in the central and normal peripheral gland was retrospectively performed, avoiding fibrous scars, cysts, and calcifications. A 20 mm^2 ROI (14 pixels) was retrospectively determined as the smallest nodule dimension in our study population.

Histopathologic Analysis

A radical prostatectomy was performed in all patients within 20 days (average 10.4 days) from the MR evaluation. After surgical resection, the prostate glands were fixed in 10% formalin. The seminal vesicles were sectioned and examined separately. The whole prostate was sectioned into 3-mm thick layers according to a plane corresponding to the axial-T2W images, to allow a precise correlation with the MRI. The sections were then embedded in paraffin and, 4 μm microsections were H&E stained.

The presence, site, and extent of the tumor was determined by a pathologist specialized in prostate pathology who was unaware of the MRI results. The tumoral lesion edges were then drawn on the slide. The histopathological analysis showed that 9 of the 30 patients had a unilateral extracapsular extension of the disease. The grading was determined according to the Gleason score.[30] The MR and histologic data analysis were finally compared and correlated.

MR Data Analysis

The overall image quality for tumor localization and local staging was assessed in a retrospective matching with the whole-mount section histopathology specimens digitally imaged by flatbed scanner.[31] MRI-detected nodules were classified as matched lesions if tumor presence and extension were evidenced at step-section histopathologic review.

The DTI images were first analyzed on the acquisition console to identify movement artifacts and image distortions correlated with eddy currents. In none of the 30 samplings were there significant misalignments connected to movement or induced currents distortions.

The data were then postprocessed with a specific software for DTI analysis and fiber tracking (FT) (PRIDE V4–Fiber Tracking 4.1, IDL, Research Systems, Boulder, CO).

When reviewing the images acquired with b factor equal to 0, (nondiffusion weighted), one of the authors of the study, in cooperation with the pathologist, positioned a 14-pixel ROI in the tumor site, directly correlating MR images and prostatectomy sections. Two ROIs of the same size were then traced on the same image in the healthy peripheral and central areas.

All the ROIs were then automatically transferred onto the corresponding mean diffusivity (MD) gray scale and fractional anisotropy (FA) maps generated by the software.

The 6 independent parts of the DTI were determined for each voxel and the eigen values (λ_1, λ_2, λ_3) of the tensor were calculated as already described by Hunsche et al.[32]

The MD [expressed in terms of apparent diffusion coefficient (ADC)] and the FA were then calculated as a mean of the values derived from each pixel inside the analyzed ROI, according to the following formulae[33]:

$$\mathrm{MD} = \lambda_m = \frac{(\lambda_1 + \lambda_2 + \lambda_3)}{3}$$

$$\mathrm{FA} = \frac{\sqrt{3}}{\sqrt{2}} \cdot \frac{\sqrt{(\lambda_1 - \lambda_m)^2 + (\lambda_2 - \lambda_m)^2 + (\lambda_3 - \lambda_m)^2}}{\sqrt{(\lambda_1^2 + \lambda_2^2 + \lambda_3^2)}}$$

Anisotropy was also visualized by generating a 24-bit RGB colorimetric map showing the magnitude of each eigen value, according to the convention that λ_1 is blue, λ_2 is red, and λ_3 is green.

This leads to the following visualization: extremely anisotropic structures that are cylindrically symmetrical ($\lambda_1 \gg \lambda_2 = \lambda_3$) appear in one color that varies from black to blue; areas with a flattened spheroid configuration (oblate regions) ($\lambda_1 = \lambda_2 > \lambda_3$) are represented with a color varying from orange to violet and finally isotropic structures ($\lambda_1 = \lambda_2 = \lambda_3$) according to a gray scale.

The structural anatomy of the prostate gland was also evaluated, showing the preferential direction of the "fibers" on a colored map [directionally encoded color (DEC)].[34]

This information was obtained on a voxel by voxel basis of the eigen vector corresponding to the largest eigen value using the scheme proposed by Jones et al[35] in which red indicates the left-right oriented "fibers", green the front to back and blue the top-bottom ones.

The tensor data were then processed with tractographic analysis according to the continuous tracking technique, as described by Mori et al.[36]

A ROI was manually traced on the non-DW images in the outline of the prostate gland. The reconstruction software then automatically made the "fibers" extraction, linking in each voxel the main eigen vector with those of the neighboring voxels. This construction produced a progressive definition of the preferential diffusivity path of the water molecules, which exactly corresponded to the "fiber" direction. To validate fiber tract depiction, reconstructions were focused on the main and well-known prostate "functional pathways" on the central gland (CG). In particular the CG was explored in all the subjects, confirming the elective radial distribution of the fibro-glandular orientation. Two sets of measurements were initially obtained on a separate sample of dogs, and the measurements were shown to be both reproducible (the means were not significantly different) and reliable (the individual values were highly correlated).

The represented "fibers" were superimposed on the non-DW images and on the DEC colorimetric maps, assigning them the directional coding color according to the previously described scheme. Finally, the fusion images were rotated across the 3 planes of the space obtaining multiplanar visualizations to delineate the relationship between the "fibers" and the anatomic structure of the gland.

The average time required for processing the diffusion tensor data, including the data transfer and the tractographic analysis was 15 minutes.

Statistical Analysis

All the quantitative data were expressed as a mean and relative standard deviation. The differences between the FA and MD resulting from the ROIs placed in the tumor lesions, the normal peripheral and central area, were calculated by two-sided Student *t* test. The statistical processing was carried out using the program for Statistical Package for Social Sciences, version 12 (SPSS, Chicago, IL). A $P < 0.05$ was considered statistically significant.

RESULTS

Thirty-four tumor nodules (≥5 mm) were identified in 30 patients. The mean nodule size was 8.4 mm (range 5–17 mm). The mean Gleason score value on postbiopsy histopathological analysis was 7 (range 5–9). Nine nodules were found as extracapsular disease in 9 patients; 25 nodules were capsule-confined in 21 patients.

For all the patients the DTI sequence image quality, retrospectively compared with the histopathology thin sec-

TABLE 1. Mean Diffusivity and Fractional Anisotropy in Patient Population

Parameter	Cancer	Peripheral Zone	Central Zone	*P*
Mean diffusivity(ADC, mm^2/s)	$1.06 \pm 0.37 \times 10^{-3}$	$1.95 \pm 0.38 \times 10^{-3}$		<0.05
		$1.95 \pm 0.38 \times 10^{-3}$	$1.59 \pm 0.40 \times 10^{-3}$	<0.05
Fractional anisotropy (FA)	0.27 ± 0.05	0.47 ± 0.04		<0.05
		0.47 ± 0.04	0.41 ± 0.08	>0.05

Values are expressed as mean ± SD.

tions, was judged to be suitable for the evaluation of the zonal anatomy of the prostate gland, clearly showing a differentiation between the normal peripheral and the central areas, with the former characterized by a higher signal and the neoplastic lesions being identifiable as focal areas of hypointensity.

A residual signal intensity, because of the lack of homogeneity of the radiofrequency, was found in relation to the bladder, but it did not affect the prostate signal.

The mean values of ADC and FA are summarized in Table 1. The Gleason score was not correlated with ADC or FA.

In the 30 patients with cancer proven by histologic analysis, quantitative evaluation of the ROIs showed a mean value of mean diffusivity (expressed in terms of ADC) that was lower in the peripheral neoplastic area ($1.06 \pm 0.37 \times 10^{-3}$ mm^2/s) than in the normal peripheral portion ($1.95 \pm 0.38 \times 10^{-3}$ mm^2/s) ($P < 0.05$) (Figs. 1 and 2).

The mean ADC values calculated in the noncancer gland regions of the central area, including benign hyperplasia, and normal peripheral area were significantly higher ($P < 0.05$) in the peripheral area ($1.95 \pm 0.38 \times 10^{-3}$ mm^2/s) than in the central area ($1.59 \pm 0.40 \times 10^{-3}$ mm^2/s).

In all cases the ADC value was significantly lower ($P < 0.05$) in the neoplastic peripheral area than in the normal central or adenomyomatous area (Fig. 2).

Quantitative evaluation of the degree of anisotropy led to results that could be partly superimposed on those relating to calculation of the ADC.

The mean FA values calculated in the normal peripheral and central areas were very similar (0.47 ± 0.04 and $0.41 \pm$

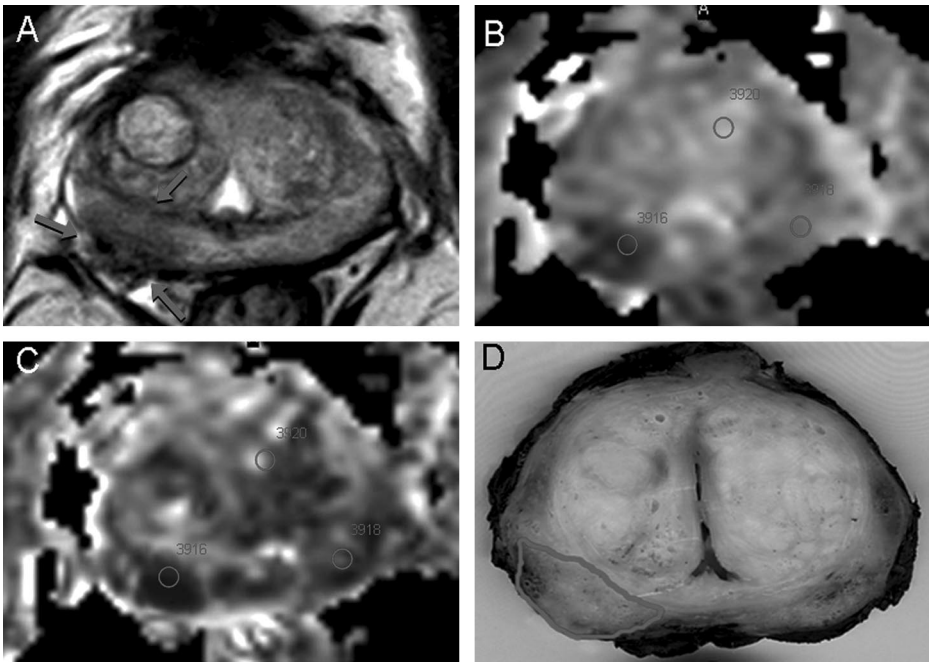

FIGURE 1. A 58-year-old patient with histologic diagnosis of adenocarcinoma (Gleason score 4 + 4) in right lobe. A, High-resolution axial-T2W TSE (TR/TE 3295/150) showing the presence of a hypointense oval area (arrows) in the right medio-lateral peripheral portion suspected for neoplastic lesion. A focal lesion "bulging," circumscribed by the anatomic capsule with consensual asymmetry of the vasculo-nervous bundle and partial obliteration of the prostate homolateral right angle, is suggestive of extracapsular extension of the disease. B, C, Same patient. DTI. Parametric map representing the degree of mean diffusivity (MD) expressed in terms of ADC (B) and map of FA (C) with the ROIs positioned in the cancer, the peripheral zone (PZ) and the central gland (CG). In the tumor a significant reduction in ADC and FA values is shown as an area of reduced signal intensity. D, The whole prostate was sectioned into 3-mm thick layers according to a plane corresponding to the axial-T2W images, to allow a precise correlation with the MR slices. The tumoral lesion edges were drawn on the slide. The MR and histologic data analysis were finally compared and correlated.

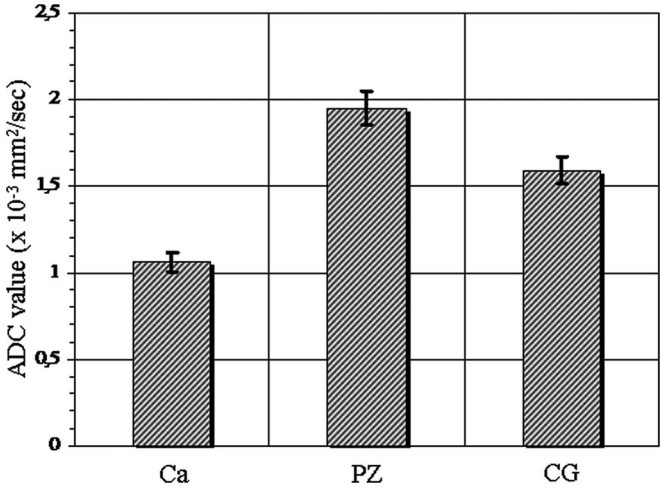

FIGURE 2. Mean ADC values in cancer (Ca), normal peripheral zone (PZ), and central gland (CG) area. Significant differences in ADC values are noted between normal and neoplastic gland and between PZ and CG.

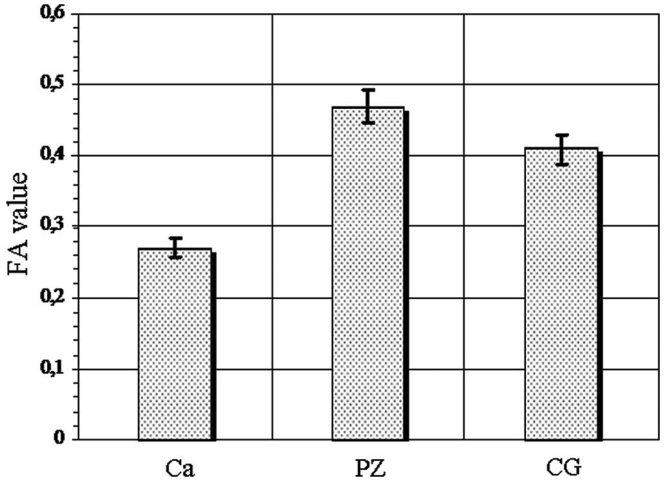

FIGURE 3. Mean FA values in cancer (Ca), normal peripheral zone (PZ), and central gland (CG) area. There are significant differences in the FA values between PZ, CG, and Ca. No statistically significant difference is noted between PZ and CG, although in the former the values are slightly higher.

0.08, respectively) and did not show a statistically significant difference between them ($P > 0.05$). The mean FA value in the neoplastic lesion (0.27 ± 0.05), on the other hand, was significantly lower ($P < 0.05$) than that calculated in the normal peripheral area and in the normal central and adenomyomatous area (Fig. 3).

The colorimetric maps relating to the degree of anisotropy showed in all the patients an intermediate grade anisotropy structure with eigen values correlated by the formula $\lambda_1 = \lambda_2 > \lambda_3$.

The reduced anisotropy in the neoplastic lesion was represented as areas with varying shades of gray. DEC-maps (Fig. 4) showed a top-bottom type preferential direction, expressed by the predominance of blue, both in the peripheral and in the central area. In the tumor lesions a reduced coding of diffusion direction was recorded, shown as noncolor gray zones.

In comparison with whole-mount sections prostate specimens tractographic analysis (Fig. 4) permitted good delineation of the prostate anatomy, correctly defining the capsule outline where the "fibers" had a top-bottom preferential direction in the middle gland portions; a front-back direction and right-left direction in the anterior apical and basal portions of the fibromuscular section. A good definition of the transition between peripheral and central area of the gland was shown in particular with the adenomyomatous hypertrophy causing a "fibers" deflection of the pseudocapsule.

The neoplastic lesions were visualized as areas of absence or reduced representation of the "fibers" determining a shift of the healthy neighboring area "fibers."

The tumor extending beyond the confines of the capsule was shown as an interruption in the representation of the "fibers" running along the outline of the anatomic capsule.

DISCUSSION

We performed a study of both normal and neoplastic prostate tissue by analyzing the DTI and its coding in tractographic processing using a 3T-MR scanner.

Diffusion tensor studies aimed at exploring the properties of anisotropy and the orientation of the "fibers" were initially carried out on the brain.

The possible applications of diffusion imaging in the prostate was partly already explored by some authors.[18,19,37,38] However, these studies were limited to the evaluation of the ADC in the different normal gland portions and in the neoplastic tissue, whereas only one work evaluated the tensor but solely in normal tissue.[22]

The benefits in terms of SNR obtained by using a magnetic field intensity of 3T compared with the 1.5T are, however, coupled with a potentiation in diffusion imaging artifacts.

Our choice of using a parallel imaging technique (SENSE technique) mitigated the 3T increased magnetic field inhomogeneity and reduced the distortions and the resolution limits dependent on the EPI single-shot acquisition technique while keeping the advantages of a reduced sensitivity to movement and a rapidity of acquisition.[29]

The use of a gated technique, that would have increased the acquisition times, was not mandatory.[22]

The mean ADC value found in the patient group in the normal peripheral and CG were substantially in agreement with previous studies.[19] The lower mean diffusivity values of the central area in respect to the peripheral one are probably an expression of the different organization of the "fibers" in the 2 gland portions: (1) the peripheral area containing muscle "fibers" loosely intersected in the abundant gland structures, (2) the central area muscle "fibers" more tightly-packed.

Our mean diffusivity values in the tumor lesion showing a significant restriction of water molecules motion was in agreement with what previously reported by Hosseinzadeh et al.[37] This restriction can be explained by analyzing the

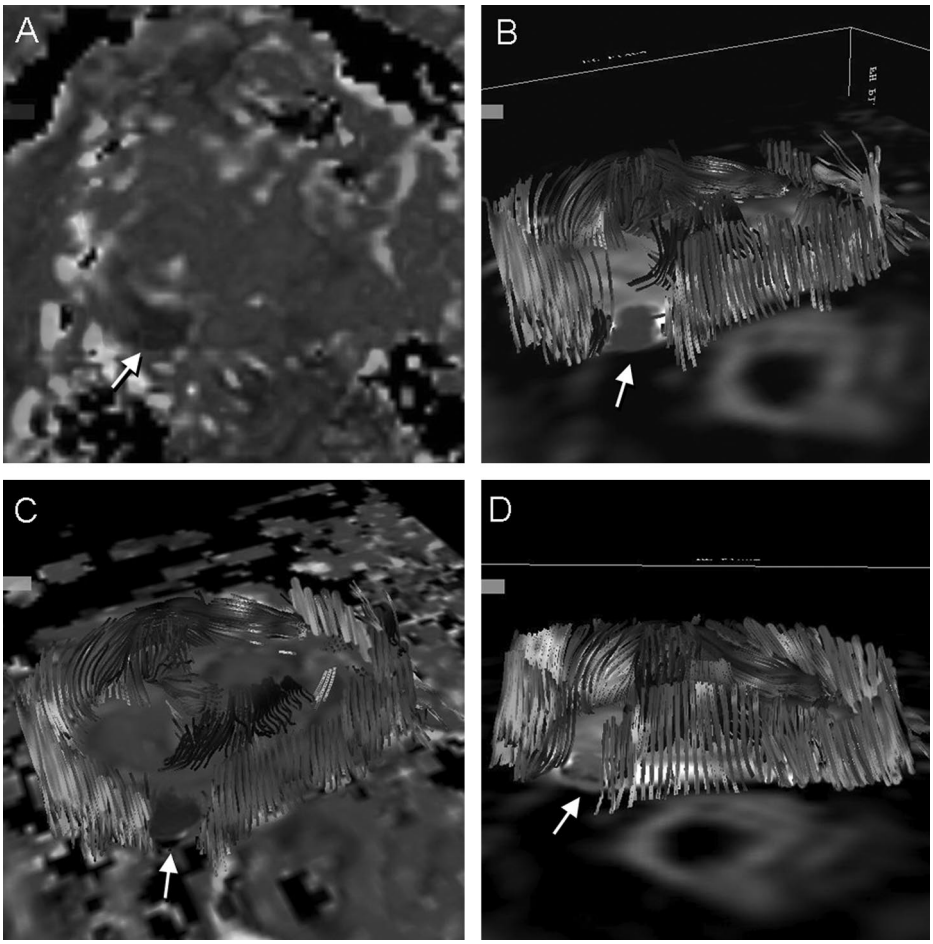

FIGURE 4. Same patient. DTI. A, The structural disorder accompanying the neoplastic lesion (arrow) determines a lack of coding in the diffusion direction of the water molecules, shown by the clear gray-black area on the coding colorimetric map of the direction of diffusivity (DEC) in the right lateral peripheral site, in accordance with the area of hypointensity present in the T2W images. B, C, D, Three-dimensional tractographic construction of the "fibers" corresponding to the diffusion movement of the water molecules that are interrupted in the neoplastic lesion (arrow). The lack of representation of the capsule outline in the tumor confirms that the neoplasia extends beyond the confines into the periprostate fatty tissue. The "fibers" are superimposed on a reference image of the diffusion sequence with value b = 0 (B, D) and on the corresponding DEC map (C). MR DTI acquisition parameters were: SE-EPI single shot sequence, TR/TE 2500/49, NSA 10, matrix 80 × 120, FOV 160 mm, in-plane voxel size 1.3 mm × 1.3 mm, b-values 2 (0, 1000 s/mm^2).

change induced by the cancer, consisting of the normal water-rich acinar components replacement with small and irregular glands, asymmetrically distributed and separated by scant connective tissue of prostate adenocarcinoma. In addition, the reduced molecular motion may be due to the increased nucleus-cytoplasm ratio in the neoplastic cells.[38]

The FA values were not significantly different in the various normal gland portions, although the peripheral area showed a trend toward slightly higher values than the central one. The FA value, like the ADC, was significantly lower in the tumor than in both the peripheral and the central area, and this could be used to distinguish normal prostate tissue from tumor tissue. Although there are no works evaluating the FA in prostate cancer, some experiments performed on brain tumors have obtained similar results concerning the changes in degree of anisotropy correlated with neoplastic degeneration. The FA values were, in fact, generally reduced in the tumor lesion compared with the surrounding healthy tissue, because of the typical structural disorder of the tumor itself. In the brain the degree of anisotropy reduction was correlated with the degree of tumor malignancy, structural disorganization, cell density inside the neoplasia, and replication activity.[39–41] Although there are substantial histologic differences with the glial tumors, a similar significance of the FA may be assumed with prostate cancer, but demonstrating this was beyond the scope of our study.

If this assumption were confirmed, the calculation of anisotropy would become another noninvasive instrument for discriminating between benign and aggressive tumor forms, making it possible to plan the most suitable therapeutic option.

Data obtained both on animal samples, and on a human population have also suggested that the calculation of the ADC could be used to evaluate the tumor response to treatment.[42]

If these findings were confirmed in prostate cancer, the ADC could be used as an evaluation parameter in the follow-up of patients undergoing conservative treatment, particularly in those on hormone therapy and for whom the PSA dose does not appear to be entirely suitable (many experimental results indicate that androgenic deprivation may inhibit the PSA independently of the block of cell growth).[43]

The DEC-map showed a preponderance of blue color, corresponding to the top–bottom direction, with some components going left-right and front-back. These findings show a correspondence in normal gland histologic organization of the central area with smooth muscle "fibers" oriented along the lengthwise axis or front-back and side

by side, following the course of the gland ducts that start radially from the prostate urethra at the verum montanum. To validate fiber tract depiction, reconstructions were focused on the main and well-known prostate "functional pathways" on the CG. In this study, we extended these observations to include the application of a fiber-tracking algorithm to a peripheral prostate gland in vivo system. In this system, the biologic structure of interest is the "prostatic lobule," which consists of connective tissue-encased, approximately circular bundles of muscle fibers with tubular-alveolar gland units, segmented by thin septa coming from the prostatic capsule, with a diameter of 300 μm in the rat and 700 μm in humans.[44] These units, oriented in the apex-base direction of the peripheral gland, are common in the fetus, usually disappear in prepuberty but reappear with age.[45]

With the in-plane resolution chosen and seed point density (1 point per voxel) we undersampled these structures. Despite this less-than-optimal spatial resolution, the excellent performance of the fiber-tracking algorithm occurs because the architecture of the adjacent "lobules" is similar enough so that they can be treated as a single structure for fiber-tracking purposes and indicates that this fiber-tracking algorithm should perform at least this well when the ratio of in-plane resolution to fiber size decreases. Tractographic representation, based on tensor data, is incapable of describing the structure of the tissue examined at cell level but the reconstructed tracts show the macroscopic configuration of the prominent "fiber" bundles.

The objective of our study was to evaluate the feasibility of tractographic processing in the prostate. The results show that it is possible to perform this evaluation in a time-range compatible with a routine MR examination. Optimization of the acquisition is essential, in particular with regard to the devices capable of reducing the distortions connected to movement that is the factor that mostly invalidates a coherent reconstruction of the "fibers."

Evaluation of the processed "fibers" showed that they correspond well with the gland anatomic structure. The prevalent "fiber" component with a top–bottom path is found in the preferential course of the smooth muscle fibrocells along the prostate lengthwise axis.

In the central adenoma, the hyperplasia of the stromal and muscular components is expressed in the formation of some well-demarcated tissue nuclei that compress the peripheral gland portion in the pseudocapsule. Tractographic representation is capable of explaining clearly this kind of change, showing in the interfaces between the hyperplasia nuclei a deflection of the "fibers" that take a circumferential path around the nuclei themselves.

In the prostate anterior outline, at the level of the fibromuscular nonglandular stromal portion, the direction of the "fibers" was shown to be prevalently side to side, in agreement with the histologic structure of this portion of the gland.

The fibrous prostate capsule is clearly delineated with mostly "fiber" components on a top-bottom path in the middle gland portions.

The scant or absence of representation of "fibers" in the neoplastic lesion shows that reduced anisotropy present in the tumor lesion determines a loss of important directional information for accurate definition of the main eigen vector and thus for 3-dimensional reconstruction of the preferential diffusivity path of the water molecules.

This result is not precisely attributable to artifacts connected to the reconstruction algorithms, because it agrees with the local ADC and FA value modifications and with anisotropy changes on the colorimetric maps in the corresponding areas.

Histologic analysis also confirmed that in the capsule outline close to the tumor region where there was no fiber representation, therefore suspected for lack of confinement of the disease, there was an extension of the tumor into the periprostatic fat. This finding seems of the utmost importance, because it is possible to assume that in the near future this type of processing might become capable of providing important information for correct tumor staging and planning treatment. The spread of the cancer beyond the capsule is the critical element in the decision to either resort to surgical treatment or to a more conservative treatment. Fiber tracking therefore is a promising instrument in evaluating the structural organization of the prostate gland.

A limit of our study, however, was the ROIs positioning performed retrospectively, in strict correlation with pathologist indications. Nevertheless nodule selection was made on the basis of digital rectal examination, T2W focal hypointensity, and a lesion diameter $\geq$5 mm. Furthermore the DTI anatomic coverage, according to the sequence we used, was about 2.61 cm thick in the base-apex long axis. As a consequence, for wider adenomas, the entire gland was not fully covered in our series.

Prostate MRI evaluation has improved during the last few years, mainly because of the introduction of endorectal coils, which significantly increase the SNR (factor of 10), enabling an accurate assessment of prostate cancer. We could not use an endorectal coil because it was not commercially available for the 3 T unit we used at the beginning of our series. But in one case, of the series presented, endorectal coil artifacts dramatically affected DTI image quality, mainly because of the patient's movement and anal contractions, making it useless for diagnosis.

The echo-time for T2 sequences (TE 150 milliseconds) that we used reduced the SNR. It was conceived to obtain the maximum T2W contrast in the peripheral zone (PZ) and a 3 T SNR spatial resolution good enough for the qualitative assessment of the hypointensity affected areas.

The correlation between MR findings and histopathology was difficult to determine in some patients, mainly because of the specimen shrinkage and deformation after fixation, so that frequently all the whole-mount section was needed for exact comparison.

Diffusion imaging currently does not enable images to be acquired with very high spatial resolution (inplane voxel size in our study: 1.3 mm $\times$ 1.3 mm). This leads to possible partial volume effects so that "fibers" with a different spatial orientation can be found inside a single voxel, reducing the information that tractographic processing is able to provide on finer structural correlations.

Finally, the quantitative comparisons of the orientation of the principal eigen vector with optical measurements of cell geometry were not performed because considered of no clinical interest.

In conclusion, our preliminary study shows that this type of functional evaluation, currently almost exclusively reserved to brain studies, can be applied to the evaluation of the prostate gland, and without a dramatic increase in MR execution times, open up very promising diagnostic and therapeutic prospects.

REFERENCES

1. American Cancer Society. *Cancer Facts and Figures 2006*. Atlanta, GA: American Cancer Society; 2006.
2. Shibata A, Whittemore AS. Prostate cancer incidence and mortality in the United States and the United Kingdom. *J Natl Cancer Inst*. 2001; 93:1109–1110.
3. Wetter A, Engl TA, Nadjmabadi DJ, et al. Combined MRI and MR spectroscopy of the prostate before radical prostatectomy. *AJR Am J Roentgenol*. 2006;187:724–730.
4. Futterer JJ, Heijmink SW, Scheenen TW, et al. Prostate cancer localization with dynamic contrast-enhanced MR imaging and proton MR spectroscopic imaging. *Radiology*. 2006;241:449–458.
5. Tanimoto A, Nakashima J, Kuribayashi S, et al. Prostate cancer screening: the clinical value of diffusion-weighted imaging and dynamic MR imaging in combination with T2-weighted imaging. *J Magn Reson Imaging*. 2007;25:146–152.
6. Miao H, Fukatsu H, Ishigaki T. Prostate cancer detection with 3T-MRI: comparison of diffusion-weighted and T2-weighted imaging. *Eur J Radiol*. 2007;61:297–302.
7. Le Bihan D, Mangin JF, Poupon C, et al. Diffusion tensor imaging: concepts and applications. *J Magn Reson Imaging*. 2001;13:534–546.
8. Bammer R, Acar B, Moseley ME. In vivo MR tractography using diffusion imaging. *Eur J Radiol*. 2003;45:223–234.
9. Dong Q, Welsh RC, Chenevert TL, et al. Clinical applications of diffusion tensor imaging. *J Magn Reson Imaging*. 2004;19:6–18.
10. Conturo TE, Lori NF, Cull TS, et al. Tracking neuronal fiber pathways in the living human brain. *Proc Natl Acad Sci USA*. 1999;96:10422–10427.
11. Geijer B, Holtas S. Diffusion-weighted imaging of brain metastases: their potential to be misinterpreted as focal ischaemic lesions. *Neuroradiology*. 2002;44:568–573.
12. Basser P, Pajevic S, Pierpaoli C, et al. In vivo fiber tractography using DT-MRI data. *Magn Reson Med*. 2000;44:625–632.
13. Murtz P, Flacke S, Traber F, et al. Abdomen: diffusion-weighted MR imaging with pulse-triggered single-shot sequences. *Radiology*. 2002; 224:258–264.
14. Chan JH, Tsui EY, Luk SH, et al. Diffusion-weighted MR imaging of the liver: distinguishing hepatic abscess from cystic or necrotic tumor. *Abdom Imaging*. 2001;26:161–165.
15. Ichikawa T, Haradome H, Hachiya J, et al. Diffusion-weighted MR imaging with single-shot echo-planar imaging in the upper abdomen: preliminary clinical experience in 61 patients. *Abdom Imaging*. 1999; 24:456–461.
16. Guo Y, Cai YQ, Cai ZL, et al. Differentiation of clinically benign and malignant breast lesions using diffusion-weighted imaging. *J Magn Reson Imaging*. 2002;16:172–178.
17. Moteki T, Ishizaka H. Diffusion-weighted EPI of cystic ovarian lesions: evaluation of cystic contents using apparent diffusion coefficients. *J Magn Reson Imaging*. 2000;12:1014–1019.
18. Gibbs P, Tozer DJ, Liney GP, et al. Comparison of quantitative T2 mapping and diffusion-weighted imaging in the normal and pathologic prostate. *Magn Reson Med*. 2001;46:1054–1058.
19. Issa B. In vivo measurement of the apparent diffusion coefficient in normal and malignant prostatic tissues using echo-planar imaging. *J Magn Reson Imaging*. 2002;16:196–200.
20. Dou J, Reese TG, Tseng WY, et al. Cardiac diffusion MRI without motion effects. *Magn Reson Med*. 2002;48:105–114.
21. Ries M, Jones RA, Basseau F, et al. Diffusion tensor MRI of the human kidney. *J Magn Reson Imaging*. 2001;14:42–49.
22. Sinha S, Sinha U. In vivo diffusion tensor imaging of the human prostate. *Magn Reson Med*. 2004;52:530–537.
23. Wieshmann UC, Krakow K, Symms MR, et al. Combined functional magnetic resonance imaging and diffusion tensor imaging demonstrate widespread modified organization in malformation of cortical development. *J Neurol Neurosurg Psychiatr*. 2001;70:521–523.
24. Witwer BP, Moftakhar R, Hasan KM, et al. Diffusion tensor imaging of white matter tracts in patients with cerebral neoplasms. *J Neurosurg*. 2002;97:568–575.
25. Pierpaoli C, Barnett A, Pajevic S, et al. Water diffusion changes in Wallerian degeneration and their dependence on white matter architecture. *Neuroimage*. 2001;13:1174–1185.
26. Damon BM, Ding Z, Anderson AW, et al. Validation of diffusion tensor MRI based muscle fiber tracking. *Magn Reson Med*. 2002;48:97–104.
27. Pierpaoli C, Jezzard P, Basser PJ, et al. Diffusion tensor MR imaging of the human brain. *Radiology*. 1996;201:637–648.
28. Bammer R, Auer M, Keeling SL, et al. Diffusion tensor imaging using single-shot SENSE-EPI. *Magn Reson Med*. 2002;48:128–136.
29. Jaermann T, Crelier G, Pruessmann K, et al. SENSE-DTI at 3T. *Magn Reson Med*. 2004;51:230–236.
30. Gleason DF, Mellinger GT. Prediction of prognosis for prostatic adenocarcinoma by combined histological grading and clinical staging. *J Urol*. 1974;111:58–64.
31. Ventura L. Creating digital images of pathology specimens by using a flatbed scanner. *Histopathology*. 2002;40:294–304.
32. Hunsche S, Moseley ME, Stoeter P, et al. Diffusion-tensor MR imaging at 1.5 and 3.0 T: initial observations. *Radiology*. 2001;221:550–556.
33. Basser PJ, Pierpaoli C. Microstructural and physiological features of tissues elucidated by quantitative diffusion tensor MRI. *J Magn Reson B*. 1996;111:209–219.
34. Basser PJ, Mattiello J, LeBihan D. MR imaging of fiber tract direction and diffusion in anisotropic tissues. In: *Proceedings of the 4th Annual Meeting of ISMRM*, New York, 1996:288.
35. Jones D, Williams S, Horsfield M. Full representation of white matter fiber direction on one map via diffusion tensor analysis. In: *Proceedings of the 5th Annual Meeting of ISMRM*, Vancouver, Canada, 1997:1743.
36. Mori S, Crain BJ, Chacko VP, et al. Three dimensional tracking of axonal projections in the brain by magnetic resonance imaging. *Ann Neurol*. 1999;45:265–269.
37. Hosseinzadeh K, Schwarz SD. Endorectal diffusion-weighted imaging in prostate cancer to differentiate malignant and benign peripheral zone tissue. *Magn Reson Med*. 2004;20:654–661.
38. Catalona WJ, Andriole GL. Tumours of the prostate gland. In: Moossa AR, Schimpff SC, Robson MC, eds. *Comprehensive Textbook of Oncology.* Vol. 2. Baltimore: Williams and Wilkins;1991:1089.
39. Mori S, Frederiksen K, van Zijl P, et al. Brain white matter anatomy of tumor patients evaluated with diffusion tensor imaging. *Ann Neurol*. 2002;51:377–380.
40. Inoue T, Ogasawara K, Beppu T, et al. Diffusion tensor imaging for preoperative evaluation of tumor grade in gliomas. *Clin Neurol Neurosurg*. 2005;107:174–180.
41. Beppu T, Inoue T, Shibata Y, et al. Fractional anisotropy value by diffusion tensor magnetic resonance imaging as a predictor of cell density and proliferation activity of glioblastomas. *Surg Neurol*. 2005; 63:56–61.
42. Dzik-Jurasz A, Domenig C, George M, et al. Diffusion MRI for prediction of response of rectal cancer to chemoradiation. *Lancet*. 2002;360:307–308.
43. Seidenfeld J, Samson DJ, Hasselblad V, et al. Single-therapy androgen suppression in men with advanced prostate: a systemic review and meta-analysis. *Ann Intern Med*. 2000;132:566–577.
44. Blacklock NJ, Bouskill K. The zonal anatomy of the prostate in man and in the Rhesus monkey (Macaca Mulatta). *Urol Res*. 1977;5:163–167.
45. Hiraoka Y, Akimoto M. Anatomy of the prostate from fetus to adult - Origin of benign prostatic hyperplasia. *Urol Res*. 1987;15:177–180.